Journal of Theoretical and Applied Physics (2020) 14:329–337
https://doi.org/10.1007/s40094-020-00389-y

RESEARCH

The effects of multiwall carbon nanotubes on the electrical characteristics of ZnO-based composites

N. Asaadi[1] · M. Parhizkar[1] · H. Bidadi[1] · S. Mohammadi Aref[1] · M. Ghafouri[2]

Received: 9 February 2020 / Accepted: 8 August 2020 / Published online: 18 August 2020

Abstract

In this experimental work, the effects of multiwall carbon nanotubes (MWCNTs) on electrical characteristics of zinc oxide–MWCNT–high-density polyethylene composite varistors have been investigated. All the samples were made at the temperature of 130 °C and pressure of 60 MPa by the hot-press method. Results show that increasing zinc oxide content in the mixture increases breakdown voltage up to 170 V, where the highest nonlinear coefficient ($\alpha \sim 13$) corresponds to the samples with 95 wt% of ZnO. Results with regard to the effects of MWCNT as an additive reveal that increasing its content from 1 to 2.5% in the composites, the breakdown voltage decreases to 50 V, but the highest nonlinear coefficient (~ 14) corresponds to the sample with 1.5% of MWCNT content. It is also revealed that, heat treatment of the sample at a constant temperature of 135 °C and different time intervals from 2 to 10 h, the sample with 6 h annealing time shows maximum breakdown voltages ($V_b = 140$ V) with the highest nonlinear coefficient (~ 14). Investigation of the potential barrier height of samples shows a complete consistency with the breakdown voltage variations. The results have been justified regarding XRD patterns and SEM micrographs of samples.

Keywords Multiwall carbon nanotube · ZnO · Composite varistor · Nonlinear coefficient

Introduction

Zinc oxide with its excellent electrical properties has played a fundamental role in different branches of physics and electronics [1, 2]. Zinc oxide has a direct bandgap of 3.37 eV at room temperature and large exciton binding energy of 60 meV which makes it suitable for a wide range of applications such as gas sensors, solar cells, photocatalysis and surge protectors [3–9]. One of the most widespread applications of ZnO is in the field of surge protector voltage-dependent devices, called varistors. A varistor is used to protect electronic circuits against excessive transient energies or overvoltages [10]. At low voltages, a varistor acts as an insulator with high resistance and linear (*I*–*V*) characteristic. When the applied voltage approaches a value known as breakdown voltage, (*I*–*V*) characteristic of the varistor becomes nonlinear and it acts like a conductor which connects electrical current to the ground [11, 12]. The quality of a varistor is specified by a parameter called nonlinear coefficient which is infinite for an ideal varistor. The best-reported value for nonlinear coefficients is ~ 50 (for ceramic ZnO-based high voltage varistors) [13]. ZnO-based varistors have some advantages such as high energy absorption capability, better thermal properties and low price [14].

The most important disadvantages of ZnO-based ceramic varistors are their high breakdown voltage, low capacitive density, complex microstructure, production process, high annealing temperature (950–1100 °C), etc. [15–17]. Some of these difficulties could be solved by changing the combination of primary materials [18–20], e.g., using a combination of ZnO and conductive polymers; this kind of varistors is called composite varistors. The significant advantages of these varistors are their simple processing route, simple microstructure, low breakdown voltage, and low fabrication temperature [21–23].

These composites are usually made of an inorganic element, e.g., silicon or ZnO, a conducting polymer, e.g.,

✉ M. Parhizkar
parhizkar@tabrizu.ac.ir

[1] Department of Condensed Matter Physics, Faculty of Physics, University of Tabriz, 29 Bahman Blvd., Imam St., Tabriz, Iran

[2] Department of Physics, Faculty of Physics, Shabestar Branch, Islamic Azad University, Shabestar, Iran

polyaniline or polypyrrole and a thermoplastic material such as high-density polyethylene (HDPE).

Carbon nanotubes (CNTs) are one of the fantastic groups of materials with a wide range of applications because of their exciting electrical, optical, and magnetic characteristics, mechanical strength, and high chemical stability [24, 25]. These characteristics introduce them as one of the most essential nanomaterials in the nanoelectronic industry [26–29].

Although there are lots of papers concerning ZnO-based ceramic varistors with different kinds of additives, the number of reports about ZnO–CNT composites are rare. According to the literature, the annealing temperature of ZnO–CNT ceramic composites is still high and above 1100 °C. For hybrid composites, it is possible to reduce annealing temperature up to 160 °C, but their nonlinear coefficient is too low (~6) for surge protection applications [24, 25].

In this study, ZnO–MWCNT-based composite varistors with a simple preparation route, i.e., single-step press method as well as low preparation temperature, are introduced. CNTs are two types; single-walled carbon nanotube (SWCNT) and multiwalled carbon nanotube (MWCNT) [30, 31].

In this study, MWCNT was used because of its high purity, homogeneous dispersion, ease of mass production, low production cost per unit, and enhanced thermal and chemical stability compared to SWCNT [32–34]. The electrical properties of the introduced components are studied as a function of ZnO and MWCNT contents. Also, the effect of the annealing time interval is studied. Among different types of polyethylene, HDPE is a commonly used thermoplastic polymer because of its high degree of crystalline structure, competitive market price, etc. [35–38]. In composite varistors, HDPE has been used due to its better mechanical stability as well as lower leakage current.

Experimental

Materials

The initial materials which were used in this study are as follows:

- ZnO powder (> 99%—Merck Chemical).
- MWCNTs (internal diameter: ~3 to 5 nm, external diameter: ~8 to 15 nm, length: ~10 o 50 µm, Research Institute of Petroleum Industry, Iran).
- HDPE (Tabriz Petrochemical Company, Iran).

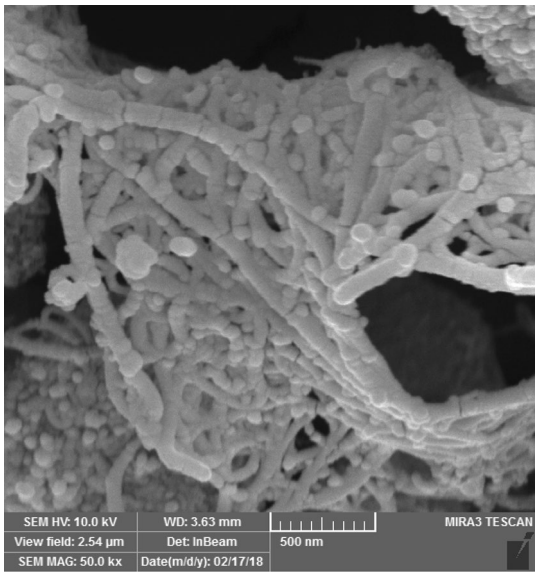

Fig. 1 SEM micrograph of MWCNTs

Table 1 Summarized information about samples with different ZnO contents and constant ratio of MWCNTs/HDPE (1:4)

No.	Sample name	ZnO content (%)	MWCNTs/HDPE content (%)
1	ZnO-85	85	15
2	ZnO-90	90	10
3	ZnO-95	95	5
4	ZnO-98	98	2

Preparation of ZnO–MWCNTs–HDPE composites

ZnO powder was milled and dried at 200 °C for 2 h. This process was repeated three times. Finally, it sifted using 200 US mesh sieve; so, the size of ZnO particles was less than 74 µm. After that, HDPE powder was also sifted with the same sieve. No specific treatment was done on MWCNTs, and it was used as it was purchased. Figure 1 shows the SEM micrograph of MWCNTs.

At the first stage, four samples with different ZnO content and constant MWCNTs/HDPE ratio (1:4) were prepared according to Table 1. At the second step, four other samples with different MWCNT content were prepared according to Table 2, where the ZnO content was constant (optimum value of ZnO according to electrical behavior).

After weighing initial materials (according to Tables 1, 2), they were mixed by magnetic balls for 10 h. All the samples were prepared by the hot-press method at the temperature of 130 °C and pressure of 60 MPa. Final samples were in a disk form with a diameter of 10 mm

Table 2 Summarized information about samples with constant ZnO content (95%) and different MWCNTs/HDPE ratios

No.	Sample name	MWCNT content (%)	HDPE content (%)
1	MWCNT-1	1	4
2	MWCNT-1.5	1.5	3.5
3	MWCNT-2	2	3
4	MWCNT-2.5	2.5	2.5

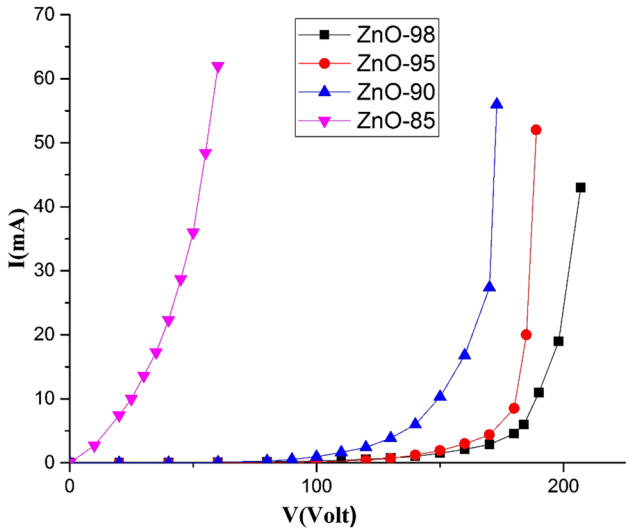

Fig. 2 (*I–V*) characteristics of samples with different ZnO contents

and thickness of 150 µm. Then, samples were annealed at the temperature of 135 °C for 6 h. To study the effect of annealing temperature on the electrical properties of samples, they were annealed at the temperature of 135 °C at different time intervals, i.e., 2, 4, 6, 8, and 10 h.

I–V characteristics of the samples were obtained by applying D.C. voltage at room temperature and measuring the current passing through them. At last, the microstructures of the composites were studied using a scanning electron microscopy (SEM), MIRA3 TESCAN system, and X-ray diffractometer D500 X-ray, Siemens Cu Kα radiation.

Results and discussion

Dependency of electrical characteristics to ZnO content

I–V characteristic of a varistor includes three regions: (a) high-resistance region (pre-breakdown region), (b) nonlinear region, and (c) low-resistance region (upturn region) [1]. Figure 2 shows *I–V* characteristics of the samples with different ZnO contents. It reveals that by increasing ZnO content of samples from 85 to 98%, their breakdown voltage increases, whereas the relevant leakage current decreases. No breakdown voltage could be defined for the ZnO-85 sample because its *I–V* characteristic tends to be linear. More decrement of ZnO content results in disappearing nonlinear behavior.

The behavior of breakdown voltage can be interpreted regarding related SEM micrographs (Fig. 3). It is clear that, by increasing ZnO content from 85 to 98%, the occurrences of two simultaneous phenomena are inevitable. First is that reducing the amount of MWCNTs at the grain boundaries decreases the conductivity of the intergranular layer which leads to a decrease in the leakage current. Second, increasing the number of ZnO grains at a constant thickness leads to an increase in the number of microvaristors between two contacts which defines breakdown voltage of the varistor according to the equation $V_B = DV_{gb}/d = NV_{gb}$, where V_B is breakdown voltage, D is thickness of the sample, d is the average grain size of ZnO, V_{gb} is voltage per grain boundary, and N is the number of microvaristors. According to the conduction theory of the varistors, breakdown voltage per microvaristor is about 3.5 V [39, 41]. So, increasing the number of microvaristors at a constant thickness will lead to an increase in the breakdown voltage which is consistent with the results given in Table 3.

In addition to breakdown voltage, the other important parameter to define a varistor is its nonlinear coefficient. *I–V* characteristic of a varistor at the nonlinear region follows Eq (1):

$$I = KV^{\alpha} \tag{1}$$

where K is a constant, V is the applied voltage, I is measured current which passes through the sample, and α is the nonlinear coefficient. So, the nonlinear coefficient of a varistor can be calculated regarding Eq (2) as the slope of the ln*I*–ln*V* curve:

$$\alpha = \left(\ln I_2 - \ln I_1\right)/\left(\ln V_2 - \ln V_1\right) \tag{2}$$

Obtained results show that by increasing ZnO content up to 95%, the value of α increases up to 13 and then decreases.

The reason for this behavior is hidden in two factors: "grain and grain boundaries" and "the intergranular layer." To study this behavior, it is sufficient to calculate the potential barrier height of the samples. Considering the conduction mechanism, it is possible to explain the effect of additives in nonlinear behavior of composites. Among different models of the conduction mechanisms, the "space-charge-limited current process in the intergranular layer with deep traps" has been proposed [13]. According to the prediction of quantum physics, the electronic wave function could penetrate the barrier if the potential barrier

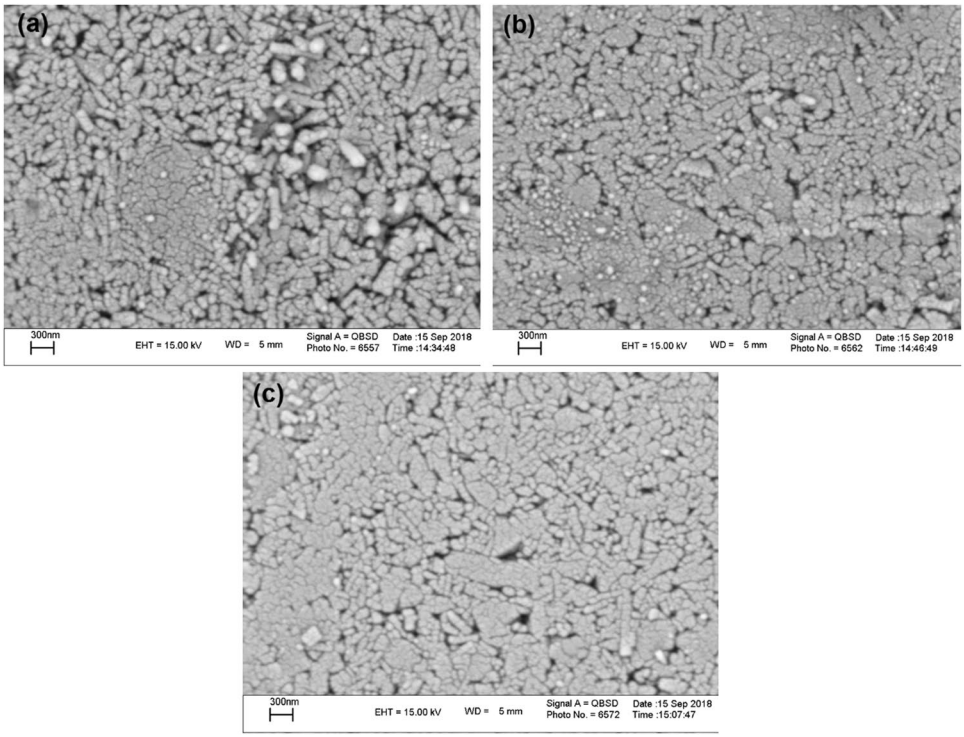

Fig. 3 SEM micrographs of the samples with different ZnO contents: **a** 85%, **b** 90% and **c** 95%

Table 3 Electrical parameters of the samples with different ZnO contents and constant ratio of MWCNTs/HDPE (1:4)

No.	Sample name	Breakdown voltage (V)	Nonlinear Coeff. (α)	Potential barrier height (eV)
1	ZnO-85	–	–	0.205
2	ZnO-90	130	7.5	0.486
3	ZnO-95	140	13	0.535
4	ZnO-98	170	10	0.395

is thin enough. Therefore, the probability of electron tunneling through the barrier is not zero. It is known as the Fowler–Nordheim tunneling mechanism which occurs above the breakdown voltage. However, below breakdown voltage, a current passing through a varistor follows the thermally activated Poole–Frenkel law or Schottky-barrier law via Eq (3):

$$I = AT^2 \exp[\left(\beta V^{\frac{1}{2}} - \varphi_b\right)/\left(k_B T\right)] \quad (3)$$

where I is the electric current, V is the electric potential difference, φ_b is the potential barrier height, k_B is the Boltzmann constant; T is the temperature, and A and β are constants. [40–43].

Calculating the potential barrier of samples (intersection of $(\ln I - \sqrt{V})$ diagram) indicates that the potential barrier height of the sample ZnO-95 has the maximum value (Table 3).

To illustrate this behavior, it should be noted that increasing ZnO content from 85 to 95% is equivalent to MWCNT decrement, so, potential barrier height increases as a result of an increase in the resistance of the intergranular layer. This phenomenon increases breakdown voltage as well. By further increase in ZnO content (up to 98%), although breakdown voltage increases, nonlinear coefficient and potential barrier height decrease.

This unconventional behavior, which is also reported for ZnO-based ceramic varistors, is a result of increases in the number of contacts between ZnO grains due to the high ZnO content (98%).

MWCNT-dependent electrical characteristics

Regarding the fact that low breakdown voltage and a high nonlinear coefficient are the main characteristics of an ideal low voltage varistor, the sample ZnO-95 with the breakdown voltage $V_B = 140$ V and $\alpha = 13$ is chosen as an optimized one to verify the effect of MWCNT content on its characteristics. Obtained I–V characteristics of samples with different MWCNT contents indicate that increasing MWCNT content in the composition causes the breakdown voltage to decrease and leakage current to increase (Fig. 4, Table 4).

Further increase in MWCNT content in the mixture raises the leakage current more severely. So, the I–V characteristic becomes linear with no definable nonlinear coefficient. By increasing MWCNT content with a constant amount of ZnO, the electrical conductivity of the intergranular layer

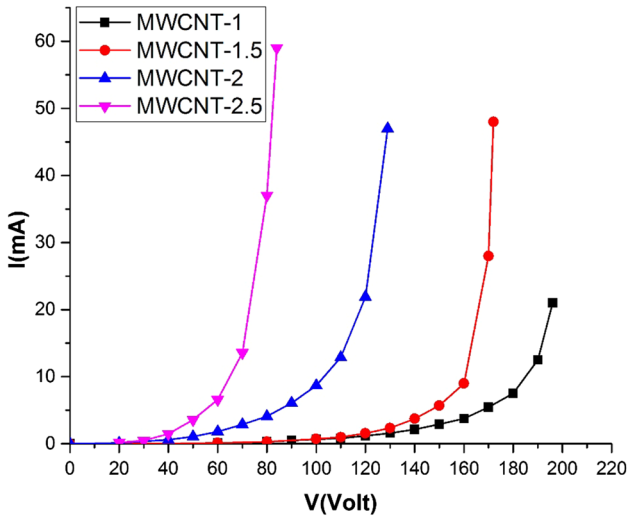

Fig. 4 (*I–V*) characteristics of the samples at constant ZnO content (95%) with different MWCNTs–HDPE ratios

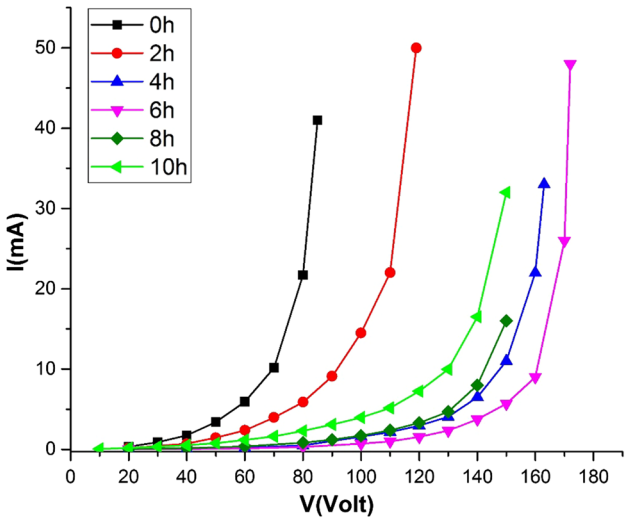

Fig. 5 (*I–V*) characteristics of the samples annealed at 135 °C for different annealing times

Table 4 The breakdown voltages and nonlinear coefficients of the samples at constant ZnO content (95%) with different MWCNTs/HDPE ratios

No.	Sample name	Breakdown voltage (V)	Nonlinear Coeff. (α)	Potential barrier height (eV)
1	MWCNT-1	170	7.2	0.38
2	MWCNT-1.5	140	14	0.39
3	MWCNT-2	90	5.5	0.36
4	MWCNT-2.5	50	4.5	0.32

Table 5 Electrical parameters of the samples at different annealing times

Sintering time (h)	Breakdown voltage (V)	Nonlinear Coeff. (α)
0	50	4.5
2	80	5.4
4	130	7.1
6	140	14
8	110	5.7
10	100	5.2

increases which results in an increase in leakage current. However, the nonlinear coefficient does not behave as breakdown voltage and leakage current by increasing MWCNT content. Among samples, the sample containing 1.5% of MWCNT has the highest nonlinear coefficient of 14. As it is discussed in Sect. 3.1, this value of α could be interpreted regarding the potential barrier height of samples (Table 4). It is obvious that by increasing MWCNT content, the values of α and φ_b will change in the same manner. For the sample MWCNT-1, the contact surface of ZnO grains is high, and its behavior looks like the sample ZnO-98. After that, the decrement of the resistance of the intergranular layer, as a result of MWCNT increment, has the main role on nonlinear coefficient and potential barrier height.

Heat treatment

In the third step, the sample ZnO–MWCNT–HDPE: 95–1.5–3.5%, with the best nonlinear behavior was chosen to undergo some heat treatments at 135 °C. This is because HDPE is approximately pasty at this temperature and surrounds other grains by time. Six samples were prepared precisely under the same condition. According to *I–V* characteristics of the samples (Fig. 5), increasing annealing time up to 6 h causes the breakdown voltage and nonlinear coefficient to increase and leakage current to decrease. After that, the phenomena become reversed (Table 5). Hence, the sample which is sintered for 6 h has the highest breakdown voltage. Calculation of nonlinear coefficient shows the same manner, i.e., the nonlinear coefficient of samples increases up to 6 h sintering interval and then decreases. Figure 6 shows the variation of breakdown voltages and related nonlinear coefficients versus annealing time interval.

This behavior of the samples is entirely justifiable considering the thermal movement of particles and SEM micrographs of samples (Fig. 7). Thermal energy makes particles to redistribute into the minimum energy. Figure 7 explicitly shows the difference between the samples without annealing, 6 h and 10 h of annealing time. For the first sample, the distribution of the particles is as "they were pressed" because of the short annealing time. However,

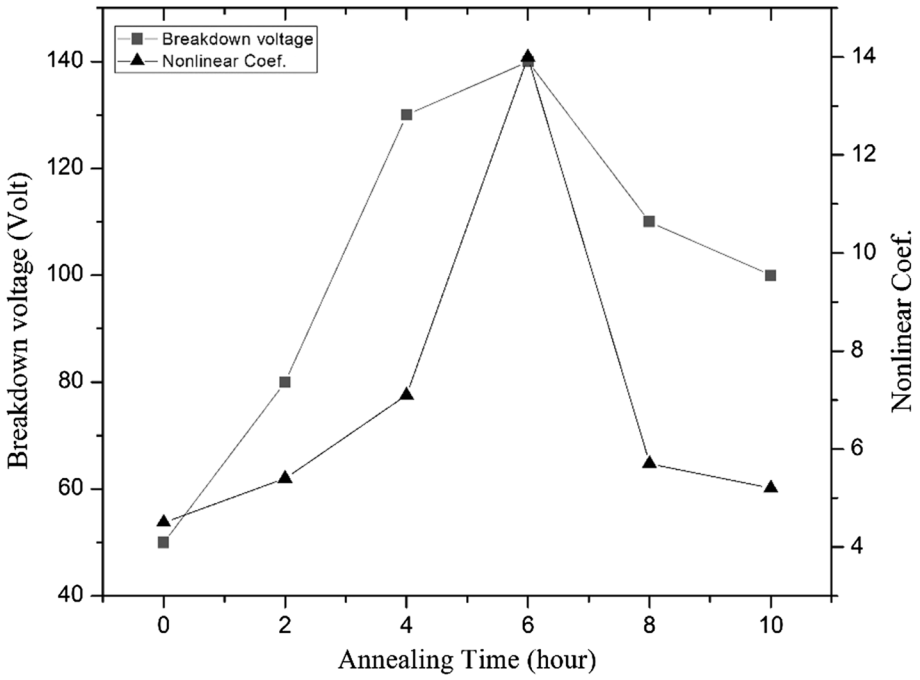

Fig. 6 Variation of breakdown voltage and related nonlinear coefficient versus annealing time

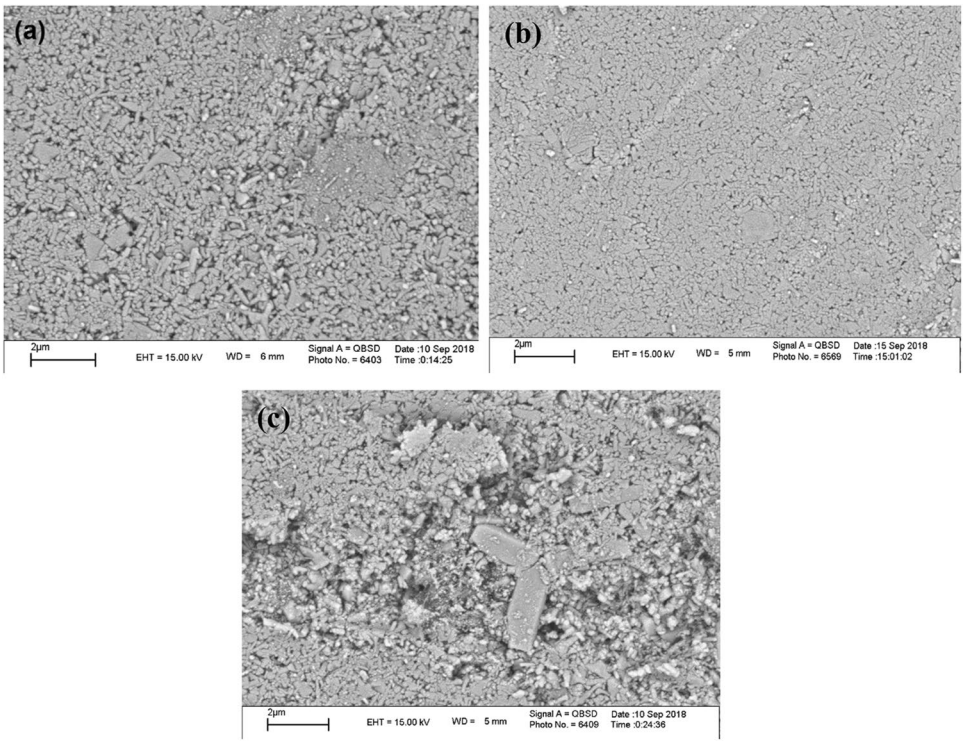

Fig. 7 SEM micrographs of samples for **a** unannealed, **b** annealed for 6 h and **c** annealed for 10 h

by increasing annealing time, particles have enough time to redistribute and the homogeneity of samples increases. This phenomenon causes the resistivity of the intergranular phase to increase which is consistent with leakage current decrement and breakdown voltages increment. Nevertheless, a further increase in annealing time destroys samples' microstructure because of the phase separation phenomenon. Phase separation is a result of the tendency of a material to aggregate together to reach minimum energy. So, the homogeneity and breakdown voltage of samples decrease, and leakage current increases.

Finally, studying XRD patterns shows all the annealed samples contain ZnO as a major phase and PE and MWCNT as a minor secondary phase (Fig. 8). It could be concluded

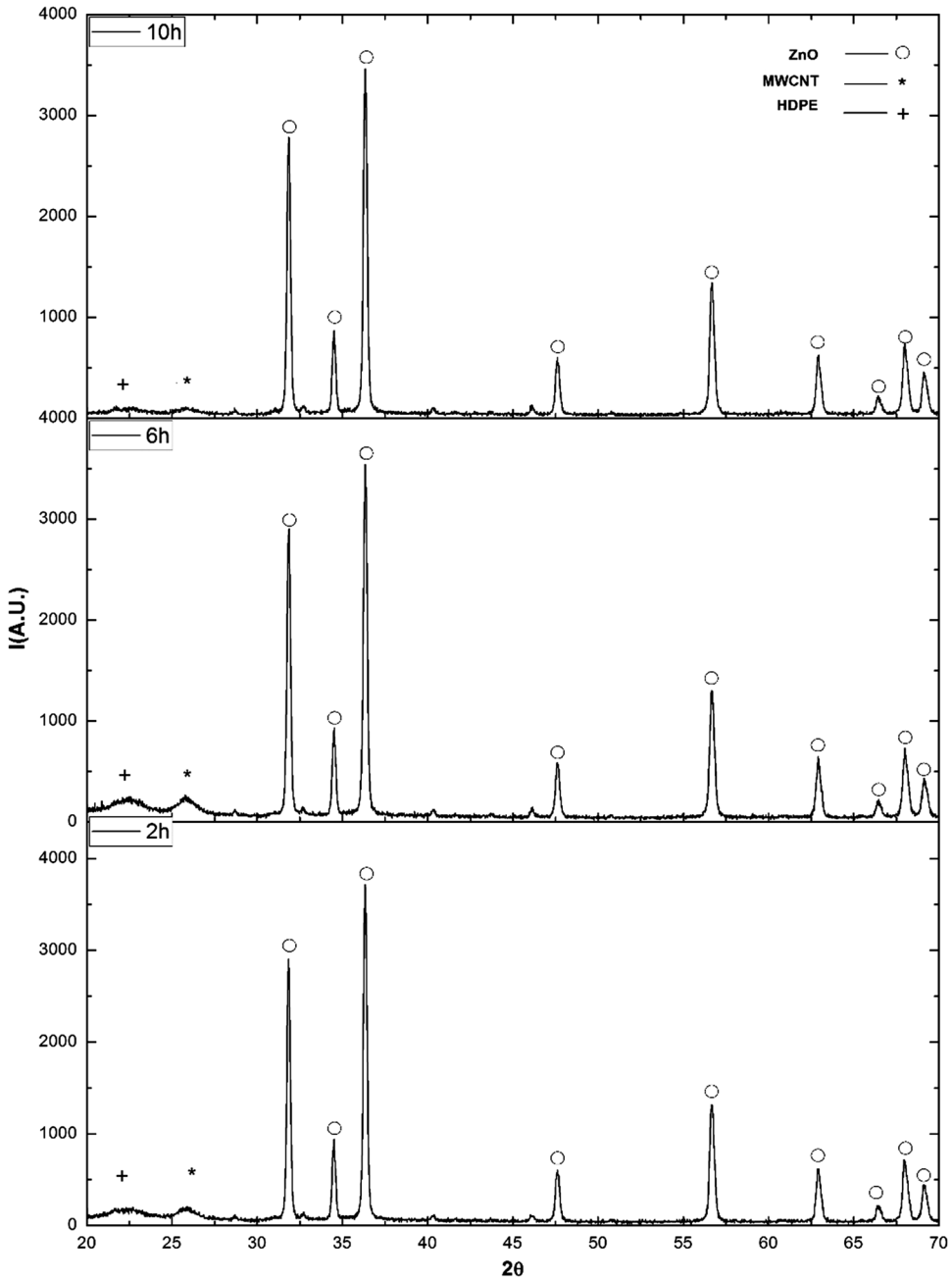

Fig. 8 XRD patterns of the samples annealed for 2 h, 6 h and 10 h

that merely the samples' grain–grain boundary microstructure is responsible for their nonlinear behaviors.

Conclusion

In this experimental work, the effects of MWCNTs content on the electrical characteristics of ZnO-based composites were studied. Results show that changing ZnO or MWCNT contents in the mixture leads to an optimum value in both breakdown voltage and nonlinear coefficient. Obtained results also show that increasing MWCNT up to 1.5% improves nonlinear coefficient. Finally, heat treatment on the sample with a mass composition of 95% ZnO and 1.5% MWCNT which is annealed for 6 h at the temperature of 135 °C, has the optimum characteristics. This sample is the best candidate to protect electrical circuits against surges and overvoltages.

Acknowledgments The financial support for this work from the University of Tabriz, Iran, is gratefully acknowledged.

References

1. Clarke, D.R.: Varistor ceramics. J. Am. Ceram. Soc. **82**, 485–502 (1999)
2. Gupta, T.K.: Application of zinc oxide varistors. J. Am. Ceram. Soc. **73**, 1817–1840 (1990)
3. Franco Jr., A., Pessoni, H.V.S.: Enhanced dielectric constant of Co-doped ZnO nanoparticulate powders. Phys. B Condens. Matter **476**, 12–18 (2015)
4. Jumidali, M.M., Hashim, M.R.: Modified thermal evaporation process using GeO_2 for growing ZnO structures. Superlattices Microstruct. **52**, 33–40 (2012)
5. Yousefi, R., Kamaluddin, B.: Dependence of photoluminescence peaks and ZnO nanowires diameter grown on silicon substrates at different temperatures and orientations. J. Alloys Compd. **479**, L11–L14 (2009)
6. Shibata, T., Unno, K., Makino, E., Ito, Y., Shimada, S.: Characterization of sputtered ZnO thin film as sensor and actuator for diamond AFM probe. Sens. Actuators A Phys. **102**, 106–113 (2002)
7. Amornpitoksuk, P., Suwanboon, S., Sangkanu, S., Sukhoom, A., Muensit, N.: Morphology, photocatalytic and antibacterial activities of radial spherical ZnO nanorods controlled with a diblock copolymer. Superlattices Microstruct. **51**, 103–113 (2012)
8. Matsubara, K., Fons, P., Iwata, K., Yamada, A., Sakurai, K., Tampo, H., Niki, S.: ZnO transparent conducting films deposited by pulsed laser deposition for solar cell applications. Thin Solid Films **431**, 369–372 (2003)
9. Vishwas, M., Rao, K.N., Gowda, K.V.A., Chakradhar, R.P.S.: Optical, electrical and dielectric properties of TiO_2–SiO_2 films prepared by a cost effective sol–gel process. Spectrochim. Acta Part A Mol. Biomol. Spectrosc. **83**, 614–617 (2011)
10. Levinson, L., Philipp, H.: ZnO varistors for transient protection. IEEE Trans. Parts Hybrids Packag. **13**, 338–343 (1977)
11. Nahm, C.-W.: Effect of sintering temperature on microstructure and electrical properties of Zn·Pr·Co·Cr·La oxide-based varistors. Mater. Lett. **60**, 3394–3397 (2006)
12. Žitnik, B., Babuder, M., Muhr, M., Žitnik, M., Thottappillil, R.: Numerical modelling of metal oxide varistors. In: Proceedings of the XIV th International Symposium on High Voltage Engineering. pp. 25–29 (2005)
13. Matsuoka, M.: Nonohmic properties of zinc oxide ceramics. Jpn. J. Appl. Phys. **10**, 736 (1971)
14. Gupta, T.K., Mathur, M.P., Carlson, W.G.: Effect of externally applied pressure on zinc oxide varistors. J. Electron. Mater. **6**, 483–497 (1977)
15. Chen, G., Yuan, C., Yang, Y.: The nonlinear electrical behavior of ZnO-based varistor ceramics with $CaSiO_3$ addition. J. Mater. Sci. **49**, 758–765 (2014)
16. Yang, Y., Zhang, X., Gao, M., Zeng, F., Zhou, W., Xie, S., Pan, F.: Nonvolatile resistive switching in single crystalline ZnO nanowires. Nanoscale **3**, 1917–1921 (2011)
17. Li, S., Li, J., Liu, W., Lin, J., He, J., Cheng, P.: Advances in ZnO varistors in China during the past 30 years—fundamentals, processing, and applications. IEEE Electr. Insul. Mag. **31**, 35–44 (2015)
18. Lee, Y., Tseng, T.: Phase identification and electrical properties in ZnO–glass varistors. J. Am. Ceram. Soc. **75**, 1636–1640 (1992)
19. Kim, E.D., Kim, C.H., Oh, M.H.: Role and effect of Co_2O_3 additive on the upturn characteristics of ZnO varistors. J. Appl. Phys. **58**, 3231–3235 (1985)
20. Hembram, K., Sivaprahasam, D., Rao, T.N.: Combustion synthesis of doped nanocrystalline ZnO powders for varistors applications. J. Eur. Ceram. Soc. **31**, 1905–1913 (2011)
21. Ghafouri, M., Parhizkar, M., Bidadi, H., Aref, S.M., Olad, A.: Effect of Si content on electrophysical properties of Si-polymer composite varistors. Mater. Chem. Phys. **147**, 1117–1122 (2014)
22. Bidadi, H., Aref, S.M., Ghafouri, M., Parhizkar, M., Olad, A.: Effect of changing Gallium arsenide content on Gallium arsenide–polymer composite varistors. J. Phys. Chem. Solids **74**, 1169–1173 (2013)
23. Aref, S.M., Olad, A., Parhizkar, M., Ghafouri, M., Bidadi, H.: Effect of polyaniline content on electrophysical properties of gallium arsenide–polymer composite varistors. Solid State Sci. **26**, 128–133 (2013)
24. Yang, W., Wang, J., Luo, S., Yu, S., Huang, H., Sun, R., Wong, C.-P.: ZnO-decorated carbon nanotube hybrids as fillers leading to reversible nonlinear *I–V* behavior of polymer composites for device protection. ACS Appl. Mater. Interfaces **8**, 35545–35551 (2016)
25. Sun, W.-J., Liu, J.-R., Yao, D.-C., Chen, Y., Wang, M.-H.: Synthesis of carbon-coated ZnO composite and varistor properties study. J. Electron. Mater. **46**, 1908–1913 (2017)
26. Dmitriev, V., Gomes, F., Nascimento, C.: Nanoelectronic devices based on carbon nanotubes. J. Aerosp. Technol. Manag. **7**, 53–62 (2015)
27. Ibrahim, K.S.: Carbon nanotubes-properties and applications: a review. Carbon Lett. **14**, 131–144 (2013)
28. Saeed, K., Khan, I.: Preparation and characterization of single-walled carbon nanotube/nylon 6, 6 nanocomposites. Instrum. Sci. Technol. **44**, 435–444 (2016)
29. Saeed, K., Khan, I.: Preparation and properties of single-walled carbon nanotubes/poly (butylene terephthalate) nanocomposites. Iran. Polym. J. **23**, 53–58 (2014)
30. Iijima, S.: Helical microtubules of graphitic carbon. Nature **354**, 56 (1991)
31. Iijima, S., Ichihashi, T.: Single-shell carbon nanotubes of 1-nm diameter. Nature **363**, 603 (1993)
32. Abrahamson, J., Wiles, P.G., Rhoades, B.L.: Structure of carbon fibres found on carbon arc anodes. Carbon N. Y. **11**, 1873–1874 (1999)
33. Hirlekar, R., Yamagar, M., Garse, H., Vij, M., Kadam, V.: Carbon nanotubes and its applications: a review. Asian J. Pharm. Clin. Res. **2**, 17–27 (2009)
34. Meyyappan, M., Delzeit, L., Cassell, A., Hash, D.: Carbon nanotube growth by PECVD: a review. Plasma Sour. Sci. Technol. **12**, 205 (2003)
35. Grigoriadou, I., Paraskevopoulos, K.M., Chrissafis, K., Pavlidou, E., Stamkopoulos, T.-G., Bikiaris, D.: Effect of different nanoparticles on HDPE UV stability. Polym. Degrad. Stab. **96**, 151–163 (2011)
36. Tanniru, M., Yuan, Q., Misra, R.D.K.: On significant retention of impact strength in clay–reinforced high-density polyethylene (HDPE) nanocomposites. Polymer (Guildf) **47**, 2133–2146 (2006)
37. Jeon, K., Lumata, L., Tokumoto, T., Steven, E., Brooks, J., Alamo, R.G.: Low electrical conductivity threshold and crystalline morphology of single-walled carbon nanotubes–high density polyethylene nanocomposites characterized by SEM. Raman spectrosc. AFM. Polym. (Guildf) **48**, 4751–4764 (2007)
38. Dilara, P.A., Briassoulis, D.: Degradation and stabilization of low-density polyethylene films used as greenhouse covering materials. J. Agric. Eng. Res. **76**, 309–321 (2000)
39. Eda, K.: Conduction mechanism of non-Ohmic zinc oxide ceramics. J. Appl. Phys. **49**, 2964–2972 (1978)

40. Levinson, L.M., Philipp, H.R.: Metal oxide varistor—a multi-junction thin-film device. Appl. Phys. Lett. **24**, 75–76 (1974)
41. Levinson, L.M., Philipp, H.R.: The physics of metal oxide varistors. J. Appl. Phys. **46**, 1332–1341 (1975)
42. Levinson, L.M., Philipp, H.R.: Conduction mechanisms in metal oxide varistors. J. Solid State Chem. Fr. **12**, 292 (1975)
43. Philipp, H.R., Levinson, L.M.: Tunneling of photoexcited carriers in metal oxide varistors. J. Appl. Phys. **46**, 3206–3207 (1975)